

Encoding method of CGH for highly accurate optical measurement based on non-maxima suppression

Xisheng Xiao (肖锡晟)^{1,2,3}, Qinghua Yu (于清华)^{1,2,*}, Zhentao Zhu (朱振涛)^{1,2,3},
Kai Hu (胡凯)^{1,2}, and Guilin Chen (陈桂林)^{1,2}

¹Shanghai Institute of Technical Physics of the Chinese Academy of Sciences, Shanghai 200083, China

²Key Laboratory of Infrared System Detection and Imaging technology, Chinese Academy of Sciences, Shanghai 200083, China

³University of Chinese Academy of Sciences, Beijing 100049, China

*Corresponding author: yuqinghua2000@126.com

Received June 20, 2017; accepted August 11, 2017; posted online August 28, 2017

The use of a computer-generated hologram (CGH) in interferometric testing provides new methods for highly accurate optical measurement. To fabricate a CGH, polygons are used to approximate the smooth CGH pattern. Because the data size supported by CGH writing machines is limited, the number of polygon vertices must be limited. Therefore, the CGH-encoding method determines the encoding accuracy. To realize a highly accurate optical measurement using CGHs, we propose a CGH-pattern-encoding method based on non-maxima suppression. A self-aligned CGH is designed to verify the accuracy. The experimental result shows that a highly accurate CGH can be fabricated using this method.

OCIS codes: 120.2880, 050.1970, 090.1760.

doi: 10.3788/COL201715.111201.

A computer-generated hologram (CGH) can generate any desired wave-front phase with diffractive light, which provides new methods for solving the problems of highly accurate optical measurement, especially in measuring complex optical surfaces^[1,2]. In recent years, CGH has proven its capability through a series of verifications and applications^[3,4].

The procedure of making a CGH includes optical design, encoding, and fabrication. The optical design can be completed using commercial optical software, and the fabrication can be completed using microelectronic technology, such as e-beam writing or laser direct writing. The encoding process can only be done by the CGH designer alone because no general method of CGH encoding is available. Most CGH studies focused on the optical design and fabrication and seldom introduced the encoding method.

The CGH-encoding process converts the desired wave-front phase function into encoded data. The format of the encoded data should be acceptable by the e-beam writing or laser direct writing machines, such as GDSII, the Caltech Intermediate Format (CIF), and the drawing exchange format (DXF)^[5]. Because the writing machines locate discrete coordinate points only, the encoded data consist of polygon vertices that approximate smooth CGH fringes. To achieve higher encoding accuracy, more polygon vertices are usually desired to approximate a smooth CGH fringe, which means high density sampling, and that leads to a huge encoding data size^[6,7]. The huge data size will not only burden the memory of the writing machine, but also take a long writing time. Therefore, to achieve high encoding accuracy with restricted data size, a proper method should be adopted while encoding the CGH pattern^[8,9].

To reduce the encoding data size while obtaining high encoding accuracy, a general encoding method of applying non-maxima suppression into the process of encoding smooth CGH fringes is introduced in this Letter. In addition, the error estimate of the method is presented. On the basis of the estimation, a self-aligned CGH is designed and fabricated to verify the accuracy of the encoding method. The experimental result is given at the end of this Letter.

After the optical design, the function of the wave-front phase generated by the CGH is expressed as $\Delta\varphi_{CGH}(x, y)$. The function $\Delta\varphi_{CGH}(x, y)$ will be encoded as a process, as shown in Fig. 1. First, a series of smooth binary fringes are generated using the phase contour interferogram method^[10], as shown in Fig. 1(a). Each contour represents wave-front phase change $m\pi$, where m is the designed diffractive order. Second, the smooth fringes are encoded into polygons that consist of segments, thus, the CGH can be fabricated by the writing machine. Figure 1(b) shows the

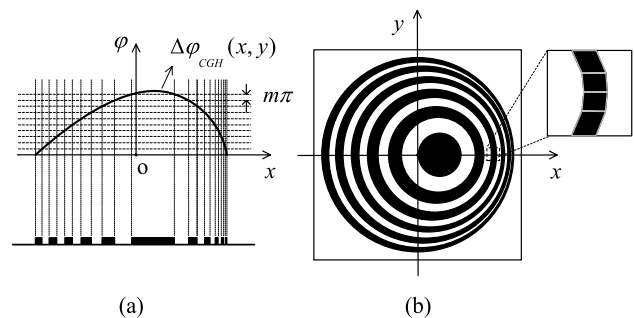


Fig. 1. CGH-encoding process. (a) Generating binary fringes using phase contour interferograms. (b) Encoding the fringes into polygons.

CGH pattern after encoding. Discrete polygon vertices are used to recode the pattern. In this study, we focus on the second step.

The CGH-encoding process inevitably introduces error to the wave-front, because any deviation from the ideal fringes leads to a wave-front phase error^[11]. Figure 2 shows the process of using a polygon to approximate an ideal smooth curve. The value of encoding deviation δ varies along the curve.

The wave-front phase error generated by the deviation is expressed as^[12]

$$\Delta W = -\frac{m \cdot \delta \cdot \lambda}{S}, \quad (1)$$

where m is the diffractive order, λ is the wavelength, and S is the local fringe spacing.

Obviously, encoding using shorter segments could reduce the encoding error. In this case, more segments are needed, and the number of vertices grows. To encode smooth CGH fringes with fewer vertices while minimizing the encoding error, the vertices of the segments should be determined according to the local curvature of the fringes, which means that the density of polygon vertices should change along the curve according to the curvature. Therefore, we propose to approximate a smooth fringe with a series of dominant points. These dominant points can rigorously represent the change of the fringe because they are the points with high local curvature. To detect these dominant points, the non-maxima suppression process based on graphic processing technology is applied in our study. The strategy below is adopted to complete the encoding process:

Step 1. Obtain the functions of the smooth CGH fringe curves, which consist of the desired CGH pattern.

Step 2. Digitalize the smooth CGH fringe curves into digital curves with high density sampling. The digitalization process should achieve a high accuracy, thus, the sampling step length should as be small as possible. Store the digital curves as temporary data.

Step 3. Apply the non-maxima suppression process to the digital curve to detect the dominant points. In this process, eliminate the points whose curvature estimates are not local maxima in a segment of the digital curve. The remaining points are the dominant points. Steps 2–3 are shown in Fig. 3. Many algorithms that originate from computer science for the graphic processing technique are available, which could be used to screen out the extrema. We choose the Teh–Chin algorithm^[13] in this study.

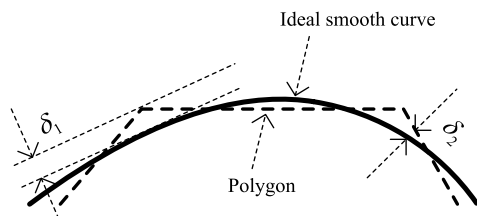


Fig. 2. Deviations introduced by encoding.

Step 4. Recode the coordinates of the dominant points in a standard exchange data format. In this study, the format of CIF is adopted.

As mentioned earlier, any process of encoding smooth fringes (or curves) inevitably introduces deviation. According to Eq. (1), any deviation can cause a wave-front error. This section provides the error estimation of our method. Figure 4 shows the digitalization of a smooth curve. Every cell in the grid is a sampling unit in the X – Y coordinate system, and the sampling step is designated as l .

Deviation occurs, whereas the curve does not change along the grid. We use δ_{sample} to represent the value of the deviation introduced by digitalization, and δ_{sample} varies within the limit,

$$\delta_{\text{sample}} < \sqrt{2}l/2. \quad (2)$$

To reduce the amount of deviation, the value of sampling step l should be as small as possible.

We define the deviation introduced by the non-maxima suppression process as suppression error δ_{suppress} . The amount of the deviation is the Euclidean distance between the digital curve and the corresponding segment of the polygon.

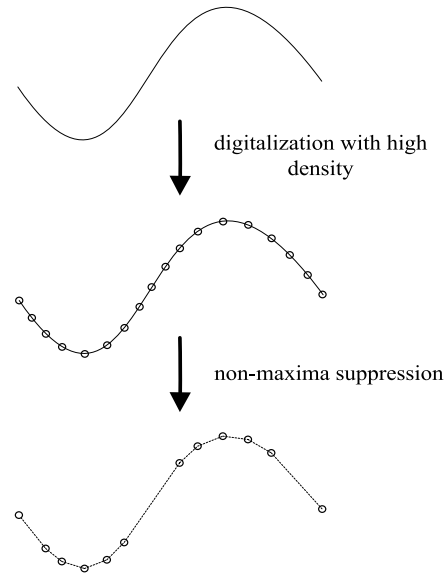


Fig. 3. Digitalization and non-maxima suppression processes.



Fig. 4. Deviation induced by digitalizing the curve.

As it shows in Fig. 5, $L_p = \{p_i, p_{i+1}, \dots, p_{j-1}, p_j\}$ is a digital curve consisting of a series of sampling points. We apply the non-maxima suppression to L_p and obtain dominant points $D_p = \{p_i, p_j\}$. The distance of the sampling point to segment $\overline{p_i p_j}$ is the suppression error δ_{suppress} of the sampling points. The algorithm adopted to screen out the dominant point determines the value of the suppression error δ_{suppress} . To verify the accuracy of the non-maxima suppression, digital curve L1 with various curvatures (sine curve) is chosen, and the result of the non-maxima suppression is shown in Fig. 6. The Teh-Chin algorithm is adopted to screen out dominant points. Suppression error δ_{suppress} induced by this algorithm is smaller than sampling step l ^[13]:

$$\delta_{\text{suppress}} < l. \quad (3)$$

The number of points on L1 is 3286, and the number of red circles, which corresponds to the detected dominant points, is 436. The data size is prominently reduced. The density of the dominant points varies according to the value of the local curvature.

We obtain δ_{suppress} of every point on L1, as shown in Fig. 7.

The horizontal axis represents the different ranges of suppression errors, whose unit is sampling step l . The vertical axis represents the number of points. Obviously, all suppression errors are smaller than l , and the value of the root mean square (RMS) suppression error is expressed as

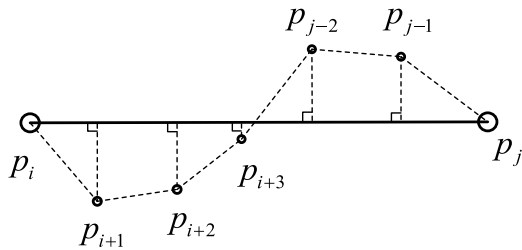


Fig. 5. Deviation induced by non-maxima suppression.

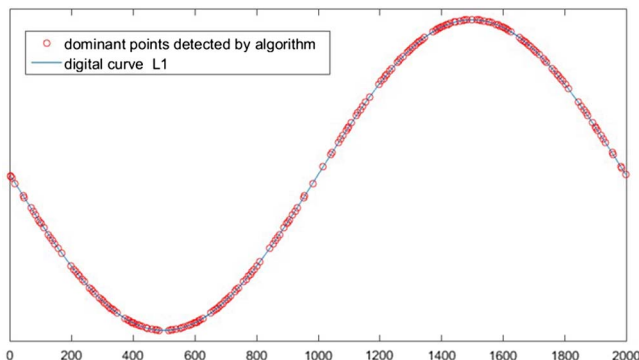


Fig. 6. Result of non-maxima suppression.

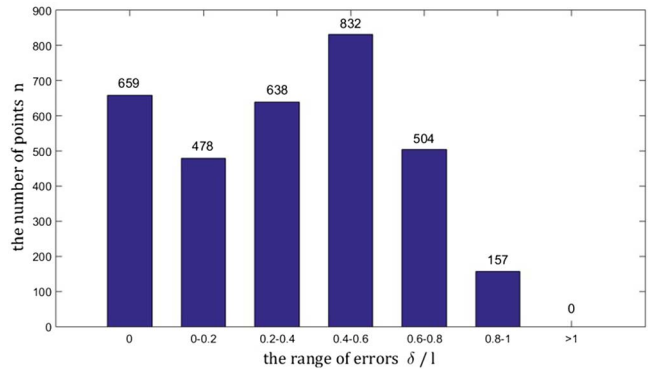


Fig. 7. Statistics of the suppression errors.

$$\text{RMS}(\delta_{\text{suppress}}) \approx 0.439l. \quad (4)$$

The sine digital curve has a typical variation in the curvature; the error estimation result of this example can verify the accuracy of the non-maxima suppression process. We estimate the maximum encoding error of our method. Steps 2 and 3 are two independent steps; add the maximum error of the steps and obtain the estimated maximum encoding error of our method by combining Eqs. (2) and (3), which is expressed as

$$\delta_{\text{encoding}} < (1 + \sqrt{2}/2)l. \quad (5)$$

According to Eq. (5), the high accuracy of the encoding process can be achieved as long as l is sufficiently small.

To verify the accuracy of the method, the interference should be suppressed. The more optical elements that are used in the measurement, the more there will be labile factors. Therefore, a type of self-aligned CGH is chosen for the experiment. Figure 8 shows the layout of the test system.

We optimize the wave-front phase function using the parameters of the surface-type Zernike fringe phase in ZEMAX. A higher diffractive order brings wider fringe spacing, which means that the writing machine can more easily plot the patterns^[12]. Therefore, a diffractive order of three is adopted in the optimization. We generate the smooth CGH fringe functions and digitalize these fringes at $l = 80$ nm. Then, we detect the dominant points on the digital fringes. Finally, we obtain the encoded data in the CIF format, whose size is 120 MB. Meanwhile, to achieve similar accuracy, the data size should reach 12.9 GB without the process of non-maxima suppression.

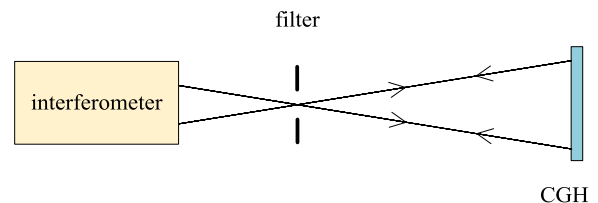


Fig. 8. Used self-aligned CGH to verify the encoding accuracy.

Figure 9 shows the layout of the CGH patterns after encoding. The pattern in the middle is the self-aligned CGH pattern. The minimum fringe spacing is 20 μm .

Considering the sensitivity to the fabrication error, the amplitude CGH is adopted to suppress interference induced by the fabrication. Similarly, the CGH pattern is directly written onto the substrate to avoid the interference induced by the process of copying the photomask pattern.

The main wave-front phase errors of our system come from the substrate error and pattern deviation. As it shows in Fig. 10, we measure the substrate error using the zero-order diffraction light, and the RMS of the substrate error is 0.012λ , where $\lambda = 632.8 \text{ nm}$. For the CGH

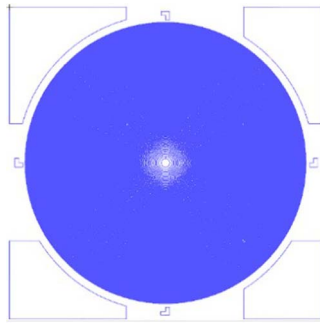


Fig. 9. Layout of the CGH.

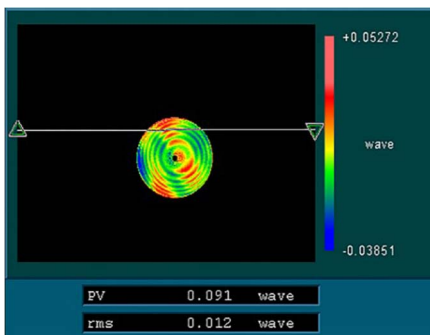


Fig. 10. Substrate error.

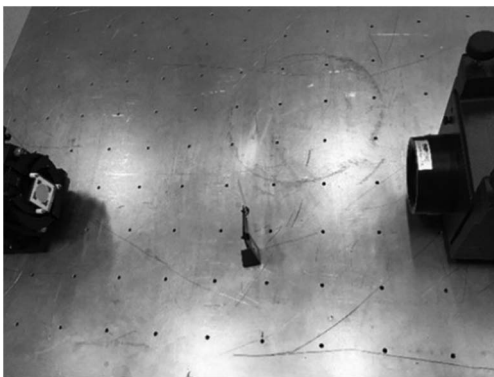


Fig. 11. Testing the reflecting wave-front generated by the CGH.

Table 1. Error Estimation

CGH Errors	Wave-front Phase Error/ λ
Substrate error	0.024
Pattern distortion error	~ 0.03
Encoding error	< 0.02
Whole path RSS error	< 0.041
Single path RSS error	< 0.0205

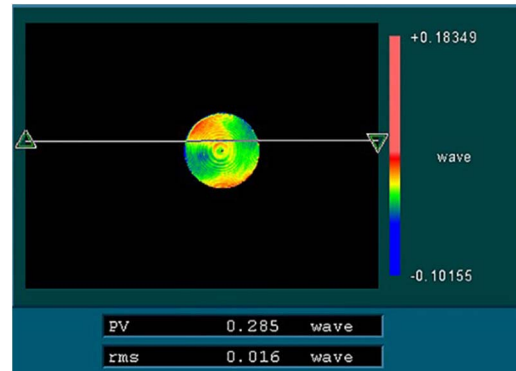


Fig. 12. Experimental result.

used as a reflecting element, the RMS of the wave-front phase error induced by the substrate error in the whole optical path is 0.024λ .

The pattern deviation includes the writing and encoding deviations. The deviation caused by the writing machine is approximately 200 nm, then the induced wave-front phase error is approximately 0.03λ , according to Eq. (1). Similarly, the estimation of the wave-front phase error induced by the encoding deviation is less than 0.02λ . The abovementioned errors are calculated in the whole optical path. Usually, the single optical path error is used to assess the accuracy of the reflecting system. We calculate the root-sum square (RSS) value of the whole optical path and obtain the estimated wave-front phase error induced by CGH, as listed in Table 1.

We measure the wave-front phase error as it shows in Fig. 11, and obtain the result in Fig. 12. The RMS of the error is 0.016λ , which is smaller than the above estimated error.

In conclusion, applying non-maxima suppression into the high accuracy CGH-encoding process is efficient. The designed diffractive order in the experiment is three, and a smaller encoding error can be achieved if a diffractive order of one is used in the optical measurement, according to Eq. (1). The experimental result shows that the CGH encoded using this method will meet the requirement of highly accurate optical measurement.

This work was supported by the Foundation of Youth Innovation Promotion Association, Chinese Academy of Sciences (No. 20150192) and the Foundation of

Innovation Program, Shanghai Institute of Technical Physics of the Chinese Academy of Sciences (No. CX-65).

References

1. T. Yang, J. Zhu, and G. Jin, *Chin. Opt. Lett.* **14**, 060801 (2016).
2. F. Zhang, *Chin. Opt. Lett.* **13**, S12202 (2015).
3. J. H. Burge, L. B. Kot, H. M. Martin, R. Zehnder, and C. Zhao, *Proc. SPIE* **6273**, 62730M (2006).
4. H. Shen, R. Zhu, Z. Gao, E. Y. B. Pun, W. H. Wong, and X. Zhu, *Chin. Opt. Lett.* **11**, 032201 (2013).
5. Z. Cui, *Nanofabrication Technologies and Applications* (Higher Education, 2005).
6. C. Zhao and J. H. Burge, in *Conference on Lasers and Electro-Optics/Pacific Rim* (2009), paper ThJ2_3.
7. I. Kallioniemi, J. Saarinen, K. Blomstedt, and J. Turunen, *Appl. Opt.* **36**, 7217 (1997).
8. J. Fan, D. Zaleta, K. S. Urquhart, and S. H. Lee, *Appl. Opt.* **34**, 2522 (1995).
9. J. Ma, Z. Gao, R. Zhu, Y. He, L. Chen, J. Li, E. Y. B. Pun, W. H. Wong, L. Huang, C. Xie, X. Zhu, and J. Ma, *Chin. Opt. Lett.* **7**, 70 (2009).
10. W. H. Lee, *Appl. Opt.* **13**, 1677 (1974).
11. W. Cai, P. Zhou, C. Zhao, and J. H. Burge, *Appl. Opt.* **52**, 8324 (2013).
12. P. Zhou and J. H. Burge, *Opt. Express* **15**, 15410 (2007).
13. C. H. Teh and R. T. Chin, *IEEE Trans. Pattern Anal. Mach. Intell.* **11**, 859 (1989).